Supplementary Information:

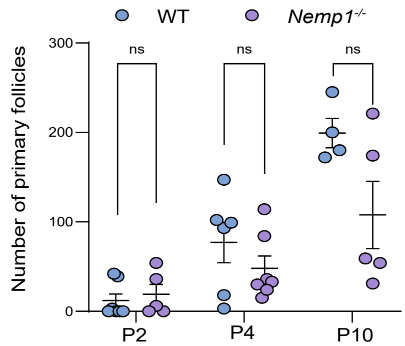

Figure S1: **Primary follicle count.** Follicle count showing a non-significant difference of primary follicles in *Nemp1$^{-/-}$* ovaries compared to wildtype (WT) at P2, P4 and P10 (ns, not significant (Unpaired t-test)), suggesting normal recruitment of primary follicles in *Nemp1$^{-/-}$* animals.

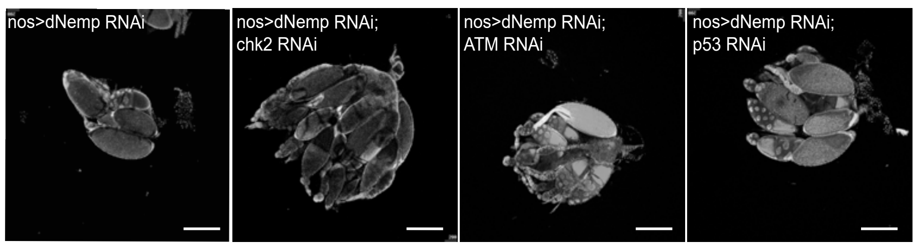

Figure S2: **ATM and Chk2 depletion rescue dNemp ovary size.** Confocal images of Drosophila ovaries dissected from 3-day-old females stained with DAPI showing relative sizes of Nemp RNAi, Nemp;Chk2 RNAi, Nemp;ATM RNAi, and Nemp;p53 RNAi ovaries (Scale Bars - 200 µm).

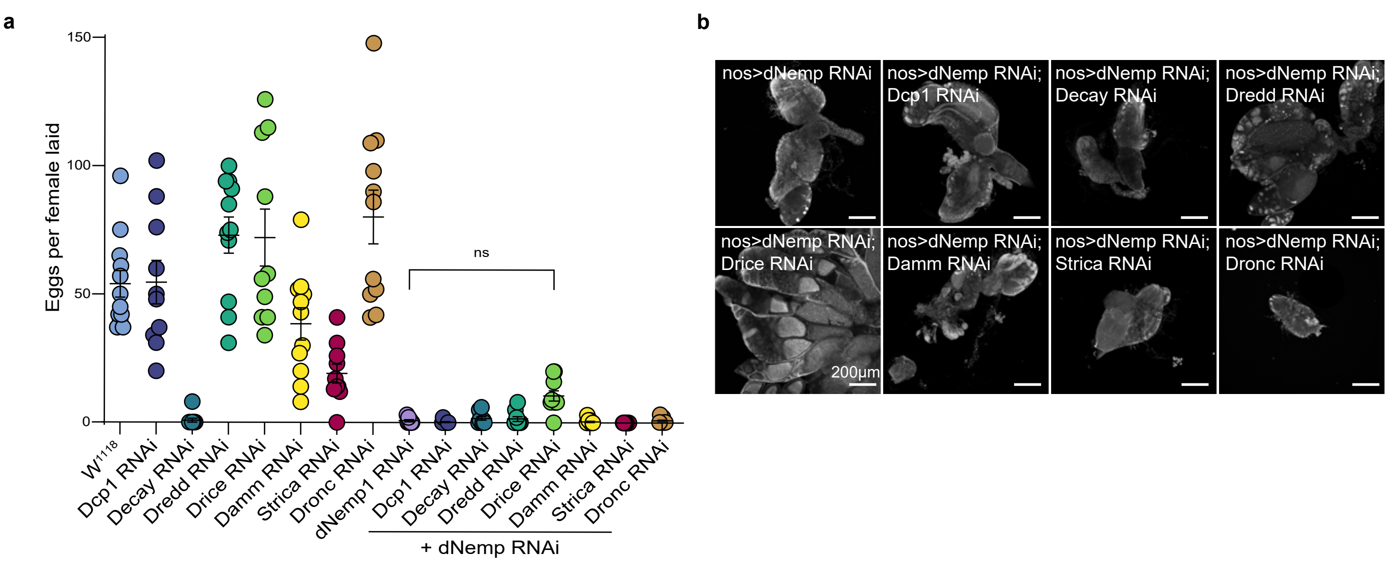

Figure S3: **Caspase depletion in dNemp ovaries.** a) The number of eggs laid by 3-day-old control (W^{1118}), single knockdown caspase mutant controls, and dNemp double knockdown caspase mutant females. ns, not significant (one-way ANOVA, Kruskal–Wallis with Dunn's multiple comparison test for nonparametric data). b) Representative confocal images of ovaries dissected from 3-day-old females showing ovary size of dNemp and dNemp double knockdown lines (Scale Bars - 200 µm).

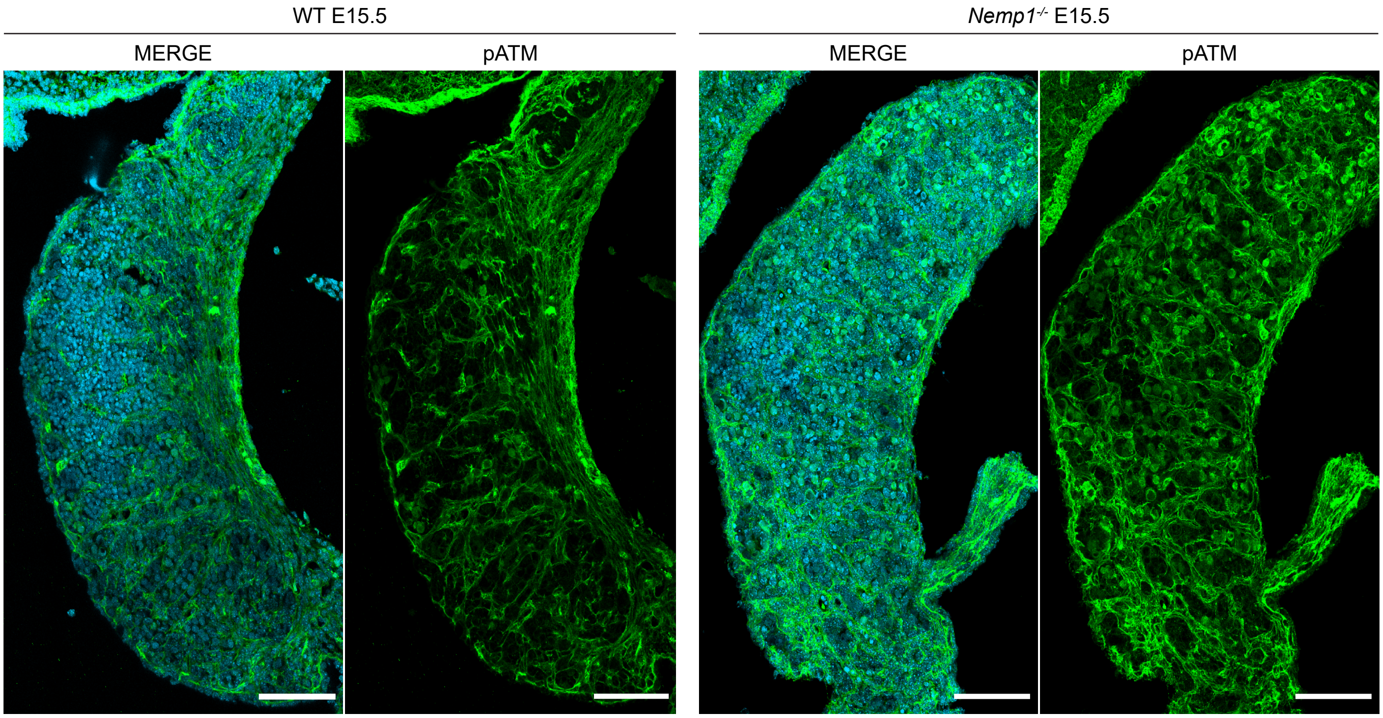

Figure S4: **ATM activation in fetal ovaries.** E15.5 ovarian cryo-section of WT and *Nemp1*$^{-/-}$ mice showing increased pATM-stained oocytes in the entire *Nemp1*$^{-/-}$ section compared to the WT (Scale Bars - 100 μm).

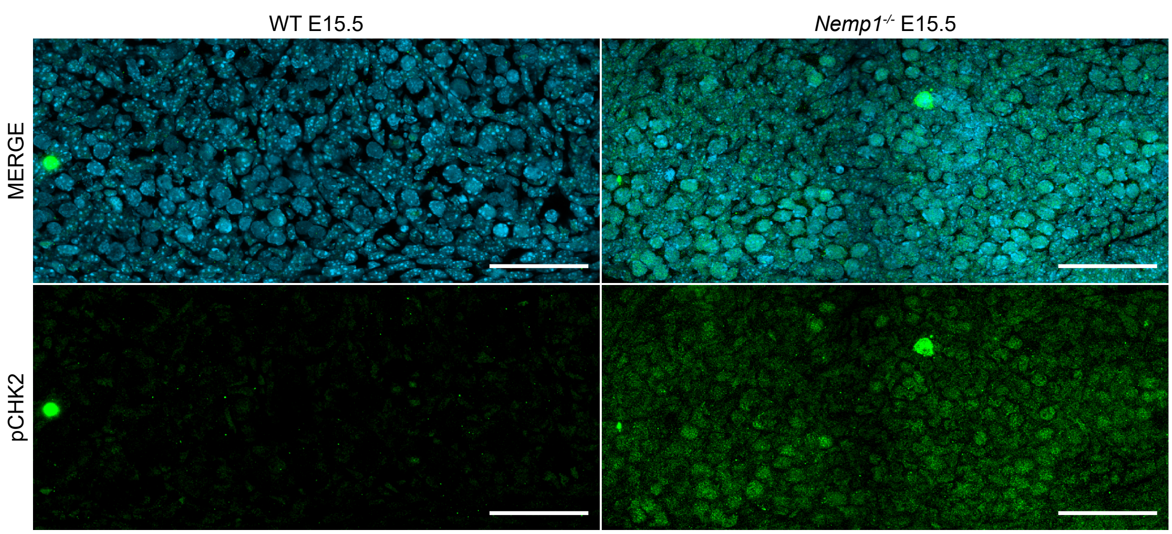

Figure S5: **CHK2 activation in fetal ovaries.** E15.5 ovarian cryo-section revealed an increased number of pCHK2-stained oocytes throughout the *Nemp1*$^{-/-}$ section than the WT (Scale Bars - 50 μm).

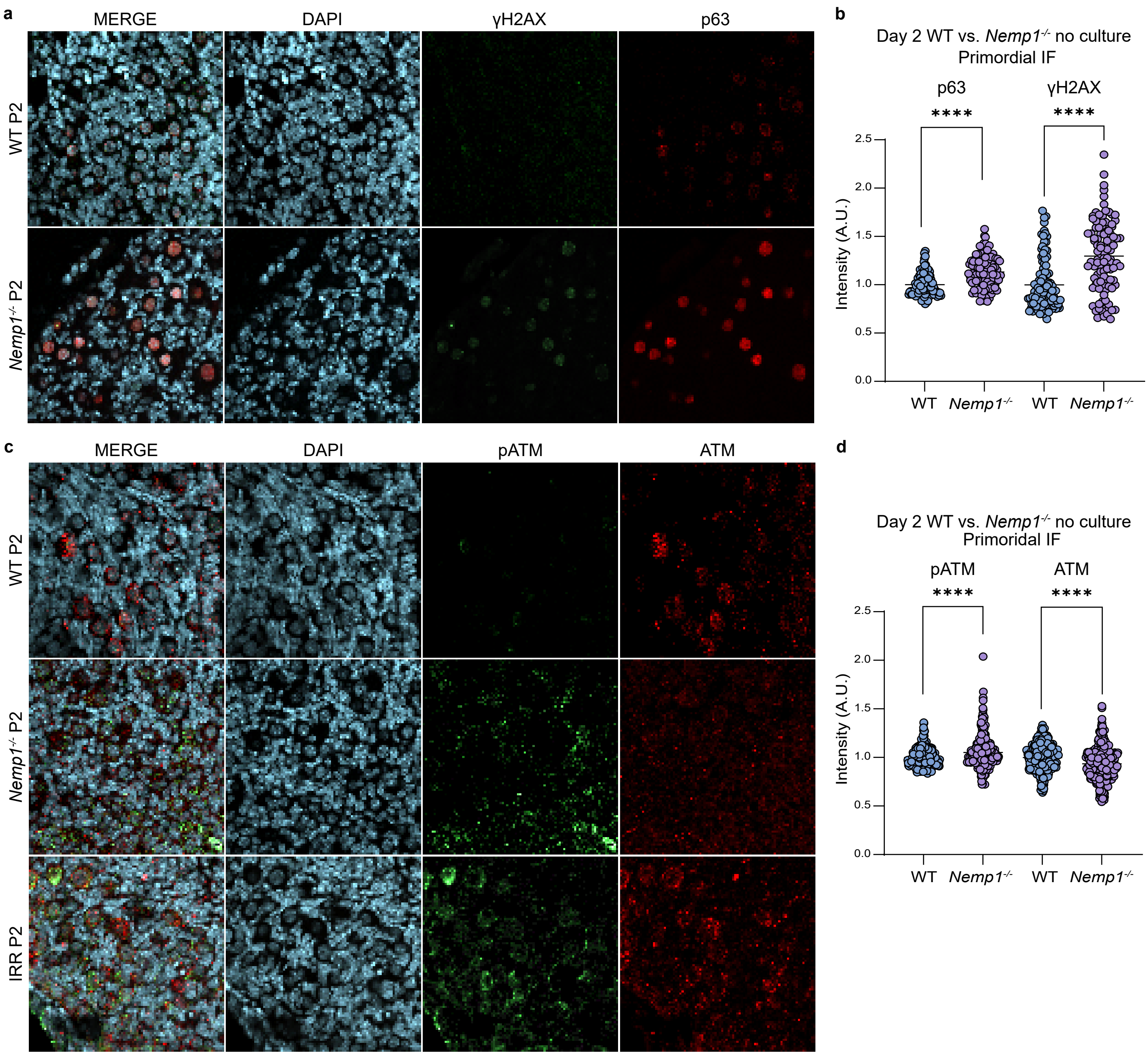

Figure S6: **Loss of Nemp1 induces DNA damage, ATM, and p63 pathway activation in post-natal ovaries.** a) Representative images of γH2ax, and p63 expression in P2 WT and *Nemp1$^{-/-}$* ovaries (Scale Bars - 50 μm). b) Quantification of γH2ax and p63 showing a significant increase in the expression of DNA damage and cell cycle checkpoint markers, respectively. ****P < 0.0001 (Mann-Whitney nonparametric test). c) Immunostaining of pATM and total ATM in P2 WT, *Nemp1$^{-/-}$ and* IRR (irradiated) ovaries (Scale Bars - 50 μm). d) Quantification of pATM and total ATM showing increased ATM activation in P2 *Nemp1$^{-/-}$* ovaries. ****P < 0.0001 (Mann-Whitney nonparametric test).

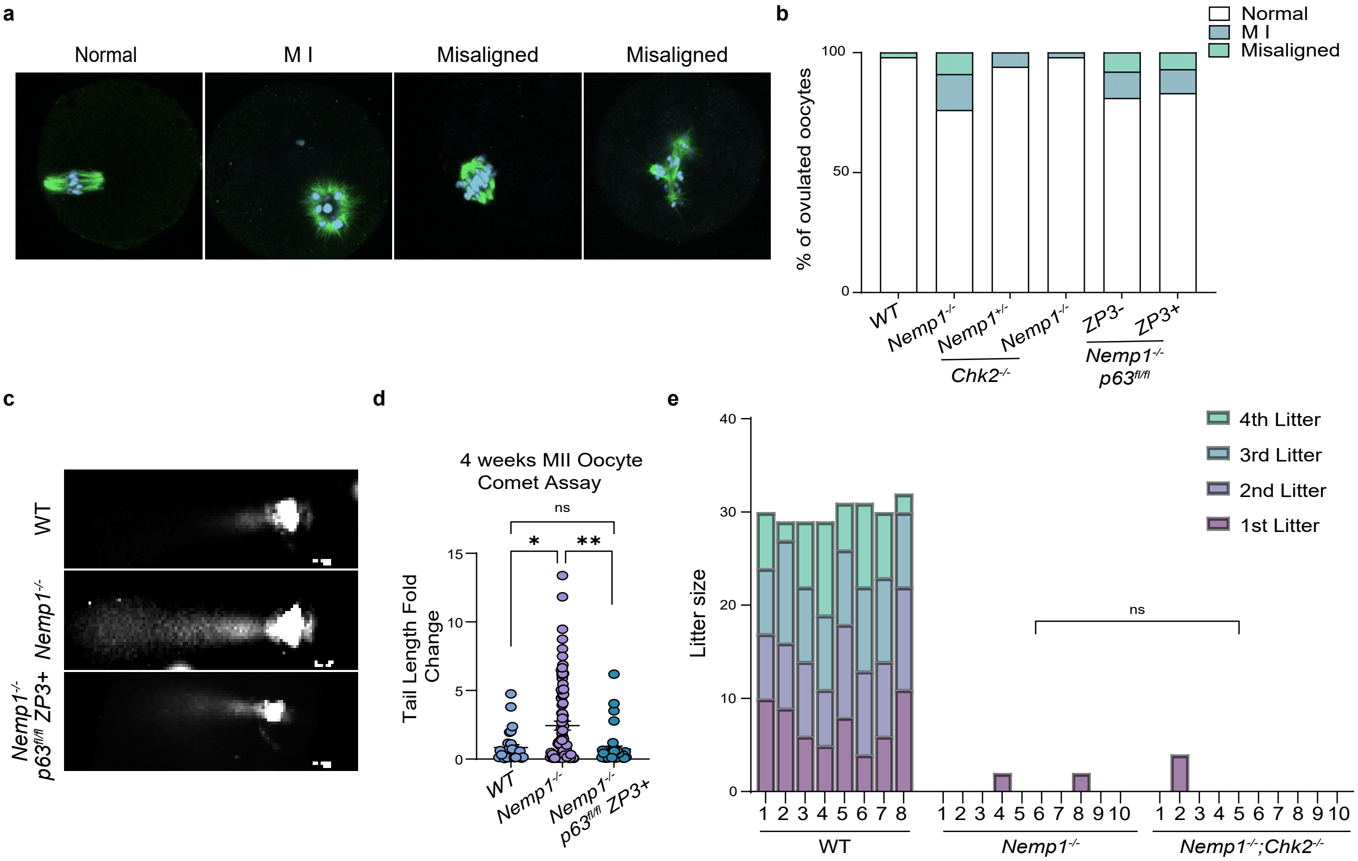

Figure S7: **Chk2 rescues spindle defects but not fertility and p63 rescues DNA damage in Nemp1 mutant MII oocytes.** a) Examples of spindle defects in *Nemp1*$^{-/-}$ ovulated oocytes. b) Proportion of various stages of ovulated oocytes shows Chk2 rescue spindle organization and chromosome alignment in mouse MII oocytes. c) Comet assay images of WT, *Nemp1*$^{-/-}$, and *Nemp1*$^{-/-}$*;p63*$^{fl/fl}$ *ZP3*+ MII oocytes (Scale Bars - 100 µm). d) Fold changes in tail moment and length in MII oocytes. (one-way ANOVA, Kruskal–Wallis with Dunn's multiple comparison test for nonparametric data). e) Litter size in control (WT), *Nemp1*$^{-/-}$, and *Nemp1*$^{-/-}$*;Chk2*$^{-/-}$ females. ns, non-significant (two-way ANOVA, Tukey's multiple comparison test).

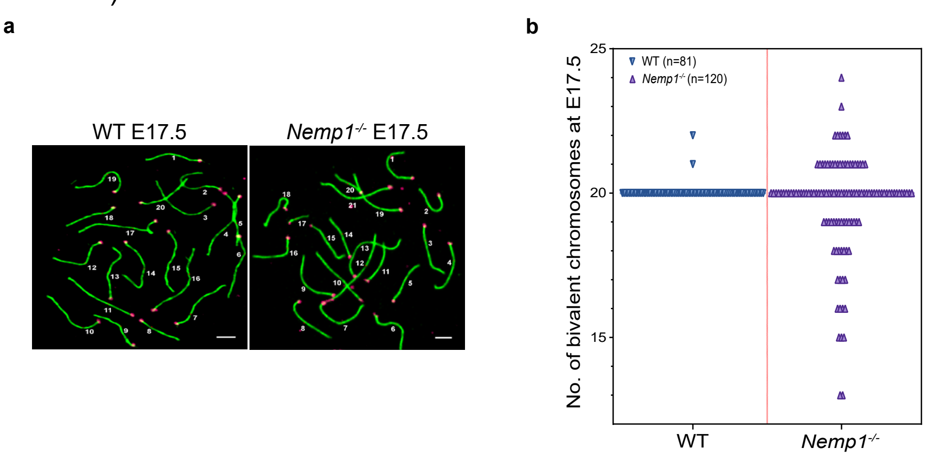

Figure S8: **Loss of Nemp1 leads to variable centromere number.** a) E17.5 chromosome spread highlighting presence of 21 centromeres in *Nemp1*$^{-/-}$ oocyte as compared with 20 centromeres (normal) in WT (Scale Bars - 5 µm). b) Quantification of bivalent chromosome number in WT and *Nemp1*$^{-/-}$ oocytes at E17.5 suggesting anueploidy in *Nemp1*$^{-/-}$ oocytes.

Supplemental Table 1: List of reagents.

Reagent	Company	Catalog Number	Comments
Rabbit anti-pChk2 (p-T68)	Bioworld Technology, Inc.	BS4043	Dilution 1:100
Mouse anti-pATM (Ser1981)	Millipore	05-740	Dilution 1:100
Rabbit anti-gamma H2A.X (pS139)	Abcam	Ab11174	Dilution 1:1000
Mouse anti-gamma H2AX (S139)	Millipore	05-636-I	Dilution 1:1000
Mouse anti-SCP3 [Cor 10G11/7]	Abcam	ab97672	Dilution 1:300
Rabbit anti-SCP1	Abcam	ab15090	Dilution 1:300
Guinea Pig anti- Hormad1	Attila Toth		Dilution 1:1000
Rabbit anti-Rad51	Millipore	PC130-100UL	Dilution 1:100
Rat anti-RPA	Cell Signaling	2208	Dilution 1:100
Mouse anti-MLH1	BD Pharmigen	550838	Dilution 1:100
Rabbit anti-DDX4 / MVH	Abcam	ab13840	Dilution 1:1000
Rat anti-GCNA1 [TRA98]	Abcam	ab82527	Dilution 1:1000
Human anti-Centromere Protein	Antibodies Inc	15-234	Dilution 1:100
alpha Tubulin (B-5-1-2), Alexa Fluor™ 488	Invitrogen	322588	Dilution 1:300
Goat anti-Rabbit IgG (H+L) Cyanine3	Invitrogen	A10520	Dilution 1:1000
Donkey anti-Rat IgG (H+L) Alexa Fluor™ Plus 647	Invitrogen	A48272	Dilution 1:1000
Donkey anti-Mouse IgG (H+L) Alexa Fluor™ Plus 488	Invitrogen	A32766	Dilution 1:800
Donkey Anti-Rabbit IgG (H+L) Rhodamine Red™-X Fab Fragment	Jackson ImmunoResearch Inc	711-297-003	Dilution 1:1000
Donkey Anti-Human IgG (H+L) Alexa Fluor® 647 $F(ab')_2$ Fragment	Jackson ImmunoResearch Inc	709-606-149	Dilution 1:500
In Situ Cell Death Detection Kit, TMR red	Sigma	12156792910	
N,N,N′,N′-Tetrakis(2-hydroxypropyl)ethylenediamine	Sigma	122262-1L	
Triethanolamine	Sigma	90279	
Urea	Fisher Scientific	U15-500	
ATM inhibitor (KU-55933)	AdooQ Bioscience	A10506	
Chk2 Inhibitor	Cayman Chemical	17552	